RSC Advances

RSC Publishing

PAPER

View Article Online
View Journal | View Issue

Cite this: *RSC Adv.*, 2013, **3**, 26438

Interfacial engineering affects the photocatalytic activity of poly(3-hexylthiophene)-modified TiO_2

Jen-Hsien Huang,[a] Mohammed Aziz Ibrahem[abc] and Chih-Wei Chu*[bd]

Received 4th July 2013
Accepted 15th October 2013

DOI: 10.1039/c3ra43393e

www.rsc.org/advances

In this study, oxidation polymerization was used to synthesize poly(3-hexylthiophene) (P3HT)-modified TiO_2 nanoparticles (NPs) and then the effect of the interface between the TiO_2 NPs and the P3HT coating on the system's photocatalytic ability under visible light was investigated. The photocatalytic properties of the TiO_2 NPs were enhanced from the UV to the visible after incorporation of P3HT. Moreover, charge transfer between the TiO_2 NPs and the P3HT coating was promoted when a self-assembled monolayer (SAM) of 2-thiophenecarboxylic acid was present at their interface; this SAM decreased the barrier for charge transfer between the TiO_2 NPs and the P3HT coating, leading to improved photocatalytic activity under visible light.

Introduction

Photocatalysis has emerged as a successful technology for purifying wastewater from industrial sources and from households. Among the many transition metal oxides that exhibit photocatalytic properties,[1–4] TiO_2 is a particularly excellent photocatalyst because of its high physical and chemical stability, low cost, high availability, nontoxicity, and unique electronic and optical properties. Nevertheless, electron–hole recombination within TiO_2 nanoparticles (NPs) leads to poor photocatalytic activity. Another issue with TiO_2 is its wide band gap (E_g > 3.2 eV), which limits the application of its particles to photocatalysis under UV irradiation only.[5]

In recent years, nanocomposites of many conductive polymers and inorganic particles have been prepared that exhibit photocatalytic responses in the visible range. The combination of TiO_2 and a conjugated polymer with suitable energy levels can lead to charge transfer between the polymer and TiO_2 and, thereby, prevent the electron and hole from recombining. Moreover, when the conjugated polymer acts as an electron donor, its photo-excitation can also produce electron–hole pairs, leading to better use of the solar light over the range from the UV to the visible. TiO_2–polyaniline,[6–10] TiO_2–polypyrrole,[11,12] TiO_2–P3HT,[13–15] and graphitic carbon(IV) nitride–polymer[16] composites can be synthesized through *in situ* oxidative polymerization—a simple, rapid method for preparing metal oxide–polymer composites on a large scale. Several problems remain to be solved, however, if we are to improve the photocatalytic activity of TiO_2 composites. The adhesion of the metal oxide to the polymer has generally been the result of physical adsorption, leading to composites having poor stability; in addition, the resistance resulting from the presence of the interface has also been large, thereby disfavoring charger transfer. Only a few researchers have investigated the effects of chemical bonding between TiO_2 and polymers on the photocatalytic activity of their composites.[6,17–19]

Direct chemical bonding of polymers onto the surfaces of TiO_2 NPs might improve the charge transfer ability and chemical stability of the resulting TiO_2–polymer composites. In this study, therefore, 2-thiophenecarboxylic acid was used to form self-assembled monolayers (SAMs) on the surfaces of TiO_2 NPs, thereby allowing subsequent surface oxidative graft polymerization to form dense P3HT layers. To investigate the effect of the SAM on the charge transfer properties, corresponding TiO_2–P3HT composites were also prepared without surface modification.

Experimental section

TiO_2–P3HT nanocomposites and dye-sensitized solar cells

TiO_2 powder was stirred in a solution of 2-thiophenecarboxylic acid (4×10^{-4} M) in $CHCl_3$ for 12 h at room temperature and then filtered off and washed with $CHCl_3$ to remove any nonbonded 2-thiophenecarboxylic acid. In a 100 mL three-necked flask, $FeCl_3$ (20 mmol) was dissolved in dry $CHCl_3$ (35 mL) under N_2. The TiO_2 powder featuring SAMs of 2-thiophenecarboxylic acid was immersed into the $FeCl_3$ solution. A solution of 3-hexylthiophene (5 mmol) in dry $CHCl_3$ (10 mL) was added dropwise; its polymerization occurred while stirring for 24 h at room temperature under N_2. Finally, the TiO_2 composite was filtered off and washed sequentially with $CHCl_3$

[a]*Department of Physics, National Taiwan University, Taipei 106, Taiwan*

[b]*Research Center for Applied Sciences, Academia Sinica, Taipei, 11529, Taiwan. E-mail: gchu@gate.sinica.edu.tw; Fax: +886-2-27826680; Tel: +886-2-27898000 ext. 70*

[c]*Nanoscience and Technology Program, Taiwan International Graduate Program, Academia Sinica, Taipei 115, Taiwan*

[d]*Department of Photonics, National Chiao-Tung University, Hsinchu, 30010, Taiwan*

(to remove any monomeric, oligomeric, and polymeric materials that had not reacted with the SAM of 2-thiophenecarboxylic acid on the TiO_2 NPs), MeOH, and deionized water (to remove residual $FeCl_3$). This sample is denoted herein as $mTiO_2$–P3HT. The procedures are displayed in Scheme 1. As a control, neat-TiO_2–P3HT composite NPs were also prepared through chemical oxidative polymerization of 3-hexylthiophene in the presence of as-received TiO_2 particles without SAM pretreatment; these composite NPs are denoted herein as TiO_2–P3HT. A thermal plastic spacer (Surlyn1702; thickness: 25 mm; Solaronix S. A., Aubonne, Switzerland) was used to seal the electrodes and control the distance between the two electrodes. The liquid electrolyte was an 3-methoxypropionitrile (MPN) solution containing 0.6 M DMPII, 0.1 M LiI, 0.05 M I_2, and 0.5 M TBP. The electrolyte was injected into the space separated by the thermal plastic spacer through a capillary effect. The Pt thin film counter electrode (CE) was sputter-deposited onto an indium tin oxide (ITO) substrate using a Cressington 108 auto sputter coater (Cressington Scientific Instruments, Watford, UK), controlled at 40 mA and 130 s.

Characterization

The morphologies of the samples were observed using scanning electron microscopy (SEM, Hitachi S-4700). Chemical compositions were confirmed through Fourier transform infrared (FTIR) spectroscopy. The structures of the TiO_2 NPs their composites were measured using X-ray diffraction (XRD). The absorption spectra of the TiO_2 composites were recorded using a UV-Vis spectrophotometer (Jasco-V-670) equipped with an integrated sphere. The photocatalytic activities of the obtained nanocomposites were evaluated by monitoring the photodegradation of methyl orange (MO) in aqueous solution; an aliquot of NPs (10 mg) was dispersed into an aqueous MO solution (2×10^{-4} M, 20 mL); while stirring, the mixed solution was irradiated for a certain period and then a portion of the solution (5 mL) was sampled and its absorbance measured. Dye-sensitized solar cells (DSSCs) were energized using a light source comprising a 450 W Xe lamp (#6266, Oriel) equipped with a water-based infrared (IR) filter and an AM 1.5 filter (#81075, Oriel). The TiO_2 and P3HT electrodes were characterized using electrochemical impedance spectroscopy (EIS) and a three-electrode system equipped with an FRA2 module in the presence of 1.0 mM redox couples and 0.1 M $LiClO_4$ in an aqueous solution; the impedance spectra were recorded at the formal potential of the redox couple in the frequency range from 0.1 Hz to 1 MHz.

Results and discussion

In this study, SAMs and the graft polymerization of 3-hexylthiophene were employed to prepare $mTiO_2$–P3HT hybrid composites. FTIR spectroscopy confirmed the chemical anchoring of the SAMs onto the TiO_2 surfaces and the subsequent polymerization of P3HT. Fig. 1 compares the FTIR absorption spectra of the TiO_2 NPs, the SAM-coated TiO_2 NPs ($mTiO_2$), and the $mTiO_2$–P3HT NPs. The absorption band of TiO_2 at 1641 cm^{-1} represents the vibration of its OH groups. The bands at 1510 and 1414 cm^{-1} of $mTiO_2$ originated from the vibrations of the carboxylate groups of the SAM,[20] indicating that 2-thiophenecarboxylic acid had been anchored successfully onto the TiO_2 NPs. For the $mTiO_2$–P3HT composite, the absorption bands of the hexyl groups and thiophene rings appeared at 2935 and 1310 cm^{-1}, respectively; these new bands provide evidence for the successful graft polymerization of 3-hexylthiophene.

UV-Vis diffuse reflectance spectra were recorded to study the optical response of the $mTiO_2$–P3HT composite. The adsorption edges of pure TiO_2 and of the TiO_2–P3HT composite appeared at 393 and 657 nm, respectively (Fig. 2a). The absorption plateau for the composite in the region 400–670 nm resulted from the presence of P3HT. Moreover, the absorption spectra of $mTiO_2$–P3HT and TiO_2–P3HT were almost identical, suggesting that the SAM had no effect on the optical properties of the composite. The band gap energies of the $mTiO_2$–P3HT nanocomposites were lower than that of the neat TiO_2 NPs, allowing the $mTiO_2$–P3HT nanocomposites to be excited to produce electron–hole pairs under visible light and, therefore, to exhibit photocatalytic

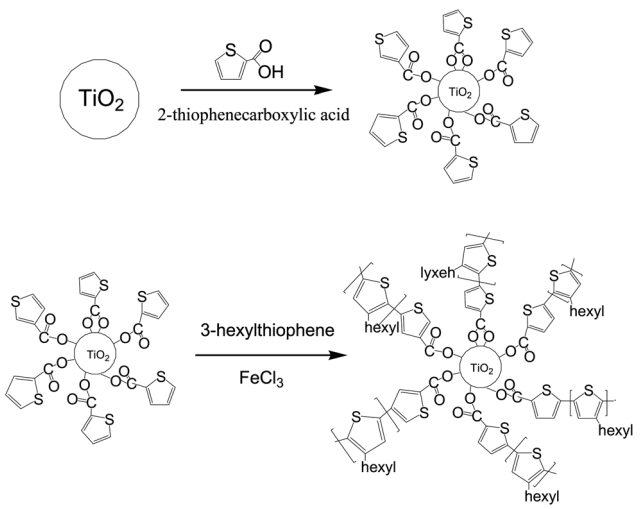

Scheme 1 Preparation of the $mTiO_2$–P3HT composite.

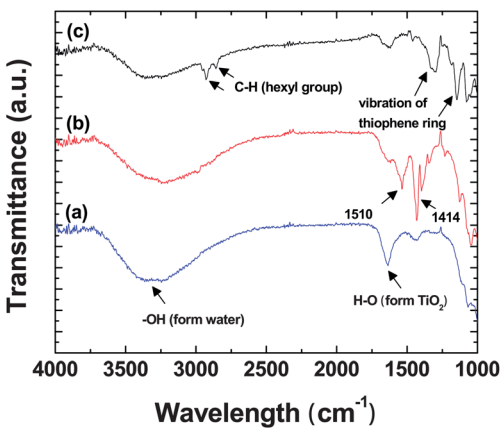

Fig. 1 FTIR spectra of (a) neat TiO_2, (b) $mTiO_2$, and (c) $mTiO_2$–P3HT.

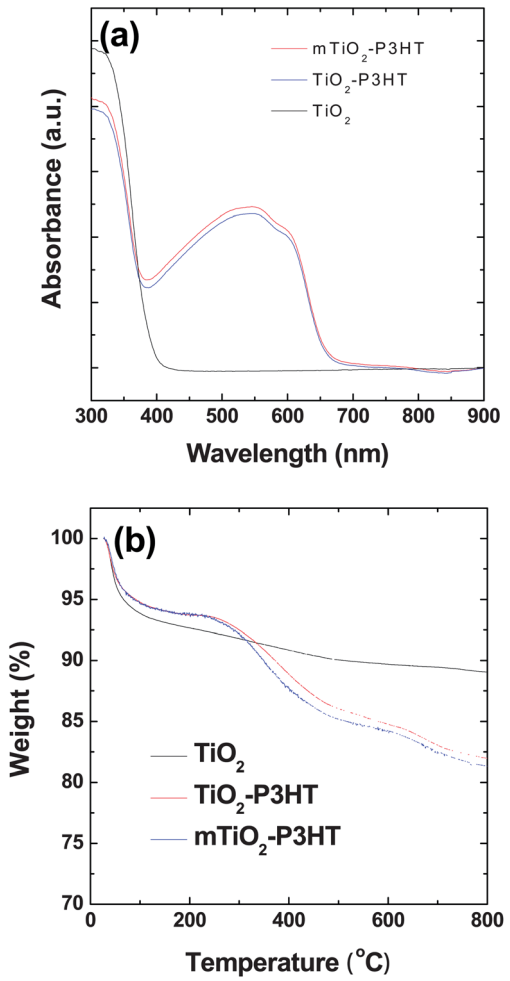

Fig. 2 (a) Absorbance spectra of neat TiO_2, TiO_2–P3HT, and $mTiO_2$–P3HT. (b) TGA curves of neat TiO_2, TiO_2–P3HT, and $mTiO_2$–P3HT.

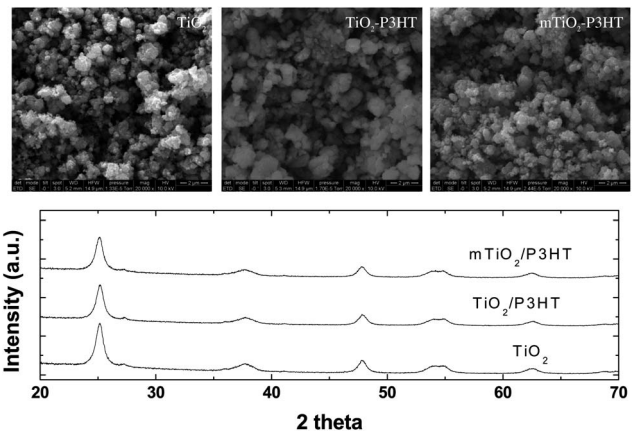

Fig. 3 SEM images and XRD patterns for neat TiO_2, TiO_2–P3HT, and $mTiO_2$–P3HT.

activity under visible light. The loading of P3HT influenced the photocatalytic activity of the nanocomposites. Although the very similar UV-Vis spectra suggested that the P3HT loadings in $mTiO_2$–P3HT and TiO_2–P3HT were similar, TGA was performed for further confirmation. Fig. 2b displays TGA curves for TiO_2, TiO_2–P3HT, and $mTiO_2$–P3HT. The weight losses at temperatures below 200 °C were due mainly to the loss of absorbed H_2O. Another stage of weight loss occurred at 310 °C, due to thermal decomposition of P3HT. TiO_2–P3HT and $mTiO_2$–P3HT both underwent weight losses of approximately 81% in the range from 30 to 800 °C. Because these two nanocomposites exhibited almost identical TGA curves, their loadings of P3HT were presumably very similar.

Because the morphologies and degrees of aggregation of the NPs will influence their specific surface areas and, therefore, their photocatalytic activities, SEM and XRD were used to investigate the structures of the neat TiO_2, TiO_2–P3HT, and $mTiO_2$–P3HT. Although all of the NPs had spherical morphologies (Fig. 3), the degree of aggregation of TiO_2–P3HT was slightly greater than those of TiO_2, and $mTiO_2$–P3HT. This behavior would presumably decrease the contact area between the TiO_2–P3HT photocatalyst and MO, leading to weaker photocatalytic activity. The XRD patterns of the prepared composites (Fig. 3) reveal that the degrees of crystallinity of the TiO_2–P3HT and $mTiO_2$–P3HT composites were lower than that of the neat TiO_2 NPs; the diffraction patterns of the composites were otherwise the same as that of the TiO_2 NPs. Therefore, the coating of P3HT on the surface of the TiO_2 NPs had no influence on the crystallization of the TiO_2 NPs.

To examine the photocatalytic efficiencies of the as-prepared powders, the photodegradation of MO under UV and visible light was investigated at room temperature. Fig. 4a displays the decreases in the concentration of MO with respect to the reaction time for photocatalysis under UV light in the presence of the various samples; all of the samples exhibited similar photocatalytic activities, with MO degrading totally after 180 min. This finding suggests that the coating of P3HT had no effect on the photocatalytic properties of the TiO_2 NPs under UV light. Under visible light (Fig. 4b), TiO_2 did not degrade MO; its concentration remained constant after 180 min of illumination. In contrast, the TiO_2–P3HT and $mTiO_2$–P3HT composites exhibited significant photocatalytic activities under visible light, presumably as a result of excitation of their P3HT units, with subsequent charge transfer between TiO_2 and P3HT expanding the range of suitable wavelengths of solar light. Hence, P3HT functioned as a sensitizer for TiO_2. After illumination with visible light for 180 min, the absorbance intensity of MO at 463 nm decreased from 0.82 to 0.47 in the presence of TiO_2–P3HT and to 0.3 in the presence of $mTiO_2$–P3HT. The greater photocatalytic activity of $mTiO_2$–P3HT was presumably due to the structure at its interface: the SAM presumably decreased the barrier for charge transfer between P3HT and TiO_2, leading to improved performance. Fig. 4c presents the UV-Vis spectra of MO recorded after various illumination times. The intensities of the signals in these spectra decreased upon increasing the irradiation time, but without any changes in their shape, suggesting that MO had decomposed completely without forming any intermediates. The results of these photocatalytic tests imply a photocatalytic mechanism under visible light that can be explained by the energy diagram in Fig. 4d. When the $mTiO_2$–P3HT composite was illuminated under

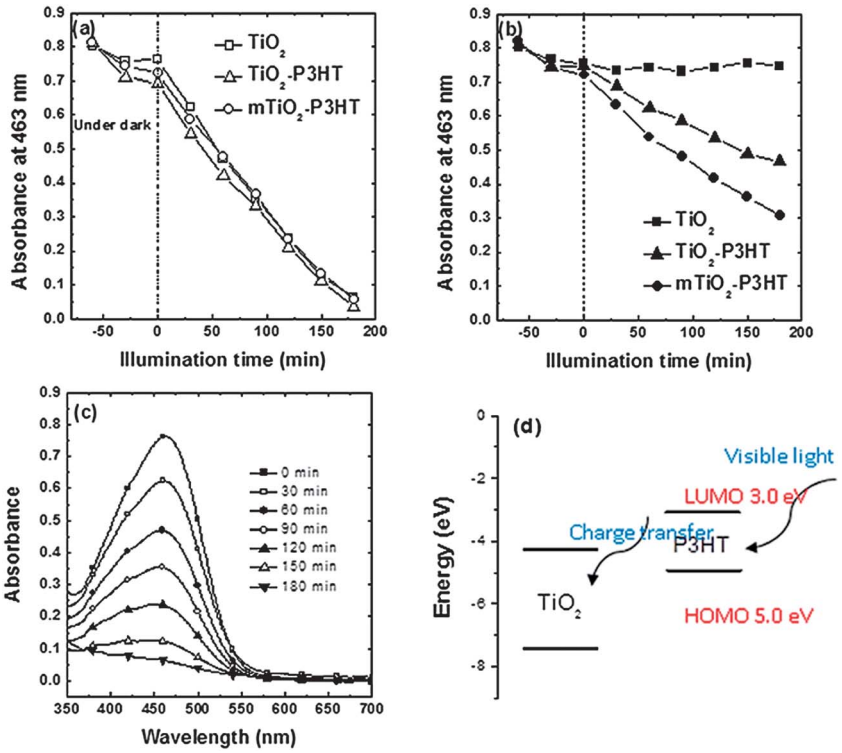

Fig. 4 (a and b) Photocatalytic degradation of MO over TiO_2, TiO_2–P3HT, and $mTiO_2$–P3HT under (a) UV and (b) visible light. (c) Absorption spectra of MO recorded after various UV illumination times. (d) Schematic energy level diagram for a composite of TiO_2 and P3HT.

visible light, both TiO_2 and P3HT absorbed the photons at their interface, where charge separation then occurred. Because the conduction band of TiO_2 and the energy level of the lowest unoccupied molecular orbital (LUMO) of P3HT are well matched for charge transfer, the electrons that were promoted through π–π* absorption of the outer P3HT film under visible light were readily injected into the conduction band of the inner TiO_2 NPs; in contrast, electrons in the valence band of TiO_2 were transferred into the P3HT, leaving holes behind. Therefore, the excited-state electrons were injected readily into the conduction band of TiO_2 and transferred to the nanocomposite surface to react with O_2 to yield superoxide radicals $\dot{O}_2^-$. At the same time, positively charged holes (h^+) were formed by electrons migrating from the TiO_2 valence band to the P3HT π-orbital; they reacted with OH^- or H_2O to generate ·OH. These two radicals, $\dot{O}_2^-$ and ·OH, were responsible for the degradation of MO. Thus, charge transfer between P3HT and TiO_2 expanded the range of solar light available for the TiO_2 photocatalyst from the UV to the visible.

To further investigate the mechanism behind the visible-light photocatalytic activity of the $mTiO_2$–P3HT composite, DSSCs incorporating $mTiO_2$–P3HT were fabricated to study the effect of P3HT on the photocurrent. Compared with the performance of the neat TiO_2 electrode, the photocurrent increased after incorporation of P3HT (Fig. 5a) as a result of excitation of the P3HT units.[21] Moreover, the DSSC incorporating $mTiO_2$–P3HT exhibited a photocurrent higher than that of the TiO_2–P3HT-containing electrode, presumably because the better quality of the interface between the TiO_2 and P3HT led to more-efficient charge transfer. This result is consistent with the tested photocatalytic activities under visible light. Fig. 5b presents the monochromatic incident photon-to-electron conversion efficiency (IPCEs) of the DSSCs. The IPCE of TiO_2–P3HT was wider than that of neat TiO_2, again due to the absorption of P3HT. Furthermore, the IPCE of $mTiO_2$–P3HT was higher than that of TiO_2–P3HT as a result of the higher quality of its interface.

To investigate the kinetics of electron transfer at the TiO_2–P3HT interface, the polymer films were characterized using EIS. Fig. 6 displays the impedance spectra of the polymer films characterized under 1.0 mM $Fe(CN)_6^{3-}/Fe(CN)_6^{4-}$ and 0.1 M $LiClO_4$ as the supporting electrolyte. The semicircle of TiO_2–P3HT is smaller than that of TiO_2, suggesting that the TiO_2–P3HT composite featured a smaller charge transfer resistance (R_{ct}) contributed from the highly conductive P3HT. Moreover, the value of R_{ct} decreased further after modification of the interface between TiO_2 and P3HT; that is, the EIS spectrum of $mTiO_2$–P3HT featured the smallest semicircle among the three tested systems. This finding is consistent with the interfacial modification promoting charge transfer between TiO_2 and P3HT, leading to a lower value of R_{ct}.

Conclusions

TiO_2–P3HT nanocomposites have been prepared through oxidative polymerization. The coating of P3HT on the TiO_2 NPs expanded the range of useable solar light from the UV to the visible. To improve the quality of the interface between TiO_2 and

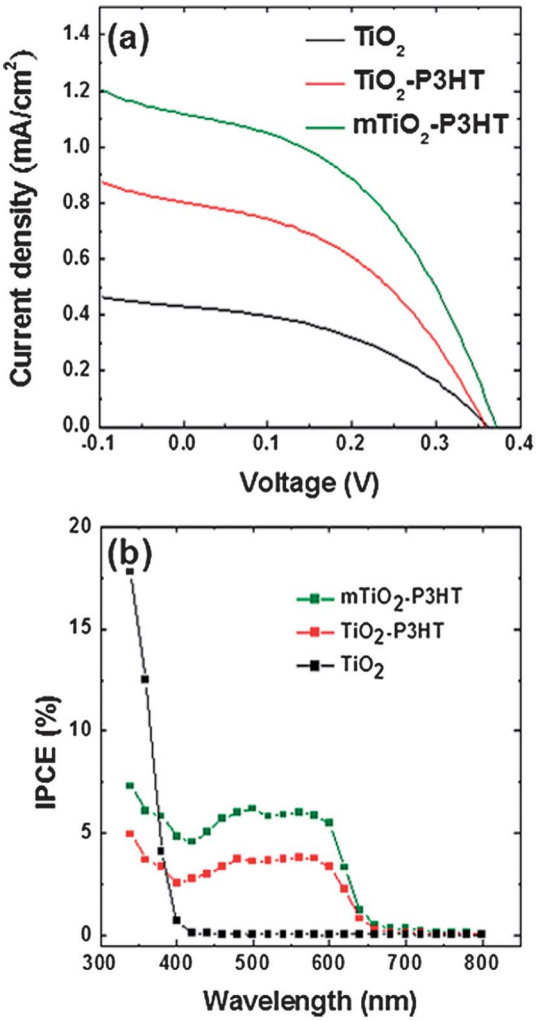

Fig. 5 (a) Performance of DSSCs incorporating TiO_2, TiO_2–P3HT, and $mTiO_2$–P3HT as electrodes; (b) corresponding IPCE curves for the DSSCs.

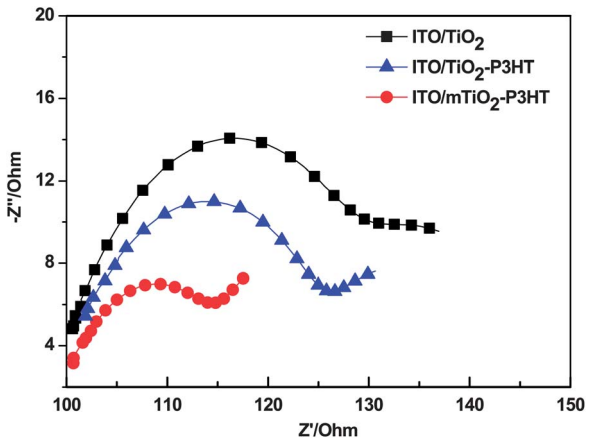

Fig. 6 EIS spectra of TiO_2, TiO_2–P3HT, and $mTiO_2$–P3HT coated on ITO substrates in 5 mM $Fe(CN)_6^{3-}/Fe(CN)_6^{4-}$ in phosphate buffer solution. Amplitude: 1 mV; frequency: 0.1 Hz to 1 MHz.

P3HT, 2-thiophenecarboxylic acid was used to form a SAM on the surface of the TiO_2 NPs. The resulting SAM-containing TiO_2–P3HT composite exhibited superior photocatalytic activity under visible light; this enhanced performance can be attributed to the lower energy barrier for charge transfer between the TiO_2 NPs and the P3HT coating.

Acknowledgements

We thank the Ministry of Education of Taiwan (through the ATU program) for financial support, National Science Council (NSC), Taiwan (NSC 102-2221-E-001-029-MY2), and the Thematic Project of Academia Sinica, Taiwan (AS-100-TP-A05), for financial support.

References

1 Y. J. Kim, B. Gao, S. Y. Han, M. H. Jung, A. K. Chakraborty, T. Ko, C. Lee and W. I. Lee, *J. Phys. Chem. C*, 2009, **113**, 19179–19184.
2 S. Y. Chai, Y. J. Kim, M. H. Jung, A. K. Chakraborty, D. Jung and W. I. Lee, *J. Catal.*, 2009, **262**, 144–149.
3 M. Saiful Rahman, M. A. Abdullah and F. K. Chong, *J. Hazard. Mater.*, 2010, **176**, 451–458.
4 J. Zhang, H. Zhu, S. Zheng, F. Pan and T. Wang, *ACS Appl. Mater. Interfaces*, 2009, **1**, 2111–2114.
5 J.-H. Huang, T.-Y. Huang, H.-Y. Wei, K.-C. Ho and C.-W. Chu, *RSC Adv.*, 2012, **2**, 7487–7491.
6 J. Li, L. Zhu, Y. Wu, Y. Harima, A. Zhang and H. Tang, *Polymer*, 2006, **47**, 7361–7367.
7 N. Wang, L. H. Zhu, J. Li and H. Q. Tang, *Chin. Chem. Lett.*, 2007, **18**, 1261–1264.
8 D. Zhao, C. Chen, Y. Wang, W. Ma, J. Zhao, T. Rajh and L. Zang, *Environ. Sci. Technol.*, 2007, **42**, 308–314.
9 Y. Lin, D. Li, J. Hu, G. Xiao, J. Wang, W. Li and X. Fu, *J. Phys. Chem. C*, 2012, **116**, 5764–5772.
10 X. Li, D. Wang, G. Cheng, Q. Luo, J. An and Y. Wang, *Appl. Catal., B*, 2008, **81**, 267–273.
11 S. S. Bhattacharya, A. Mishra, D. Pal, A. K. Ghosh, A. Ghosh, S. Banerjee and K. K. Sen, *Polym.-Plast. Technol. Eng.*, 2012, **51**, 878–884.
12 N. C. Strandwitz, Y. Nonoguchi, S. W. Boettcher and G. D. Stucky, *Langmuir*, 2010, **26**, 5319–5322.
13 D. Wang, J. Zhang, Q. Luo, X. Li, Y. Duan and J. An, *J. Hazard. Mater.*, 2009, **169**, 546–550.
14 G. Liao, S. Chen, X. Quan, H. Chen and Y. Zhang, *Environ. Sci. Technol.*, 2010, **44**, 3481–3485.
15 B. Muktha, D. Mahanta, S. Patil and G. Madras, *J. Solid State Chem.*, 2007, **180**, 2986–2989.
16 Y. Zhang, Z. Schnepp, J. Cao, S. Ouyang, Y. Li, J. Ye and S. Liu, *Sci. Rep.*, 2013, **3**, 2163.
17 S. Lu, S.-S. Sun, X. Jiang, J. Mao, T. Li and K. Wan, *J. Mater. Sci.: Mater. Electron.*, 2010, **21**, 682–686.
18 G. Xiao, Y. Wang, J. Ning, Y. Wei, B. Liu, W. W. Yu, G. Zou and B. Zou, *RSC Adv.*, 2013, **3**, 8104–8130.
19 M. D. Hernandez-Alonso, F. Fresno, S. Suarez and J. M. Coronado, *Energy Environ. Sci.*, 2009, **2**, 1231–1257.
20 Q. Qu, H. Geng, R. Peng, Q. Cui, X. Gu, F. Li and M. Wang, *Langmuir*, 2010, **26**, 9539–9546.
21 T.-H. Lee, D. Sun, X. Zhang, H.-J. Sue and X. Cheng, AVS, 2009, pp. 3073–3077.